

# Bounds on ALP-Mediated Dark Matter Models from Celestial Objects

---

Tanech Klangburam<sup>a,b</sup> Chakrit Pongkitivanichkul<sup>a,b</sup>

<sup>a</sup>*Khon Kaen Particle Physics and Cosmology Theory Group (KKPaCT),  
Department of Physics, Faculty of Science, Khon Kaen University, 123 Mitraphap Rd.,  
Khon Kaen, 40002, Thailand*

<sup>b</sup>*National Astronomical Research Institute of Thailand, Chiang Mai 50180, Thailand*

*E-mail:* [klangburam.t@gmail.com](mailto:klangburam.t@gmail.com), [chakpo@kku.ac.th](mailto:chakpo@kku.ac.th)

**ABSTRACT:** We have studied the signals from axion-like particles (ALPs) as dark matter mediators from celestial objects such as neutron stars or brown dwarfs. We consider the accumulation of dark matter inside the celestial objects using the multiscatter capturing process. The production of ALP from the dark matter annihilation can escape the celestial object and decay into gamma-ray and neutrinos before reaching the Earth. We investigate our model using gamma-ray observations from Fermi and H.E.S.S and neutrino observations from IceCube and ANTARES. The effective Lagrangian approach allows us to place constraints on the ALP-photon and ALP-fermion couplings. In the gamma-ray channel, our results improve the existing bounds on ALPs by 1-2 orders of magnitude. Although the constraints from neutrino fluxes rule out a significant portion of the parameter space, the remaining part of the parameter space is accessible by future experiments.

---

## Contents

<b>1</b>	<b>Introduction</b>	<b>1</b>
<b>2</b>	<b>Dark Matter Simplified Model</b>	<b>2</b>
<b>3</b>	<b>Dark Matter Multiscatter Capture</b>	<b>4</b>
<b>4</b>	<b>The Galactic Center</b>	<b>6</b>
<b>5</b>	<b>Detection</b>	<b>7</b>
<b>6</b>	<b>Results</b>	<b>11</b>
<b>7</b>	<b>Conclusion</b>	<b>13</b>

---

## 1 Introduction

After decades of searching for Dark Matter (DM), the models in which DM interacts directly with the Standard Model (SM) particles are strongly disfavoured. In particular, the parameter space of the standard WIMP (Weakly Interacting Massive Particle) models has been severely constrained. This has slowly led to a great interest in models with DM interactions via mediators such as Higgs portal model, neutrino portal model, etc [1–6]. Among them, one particular model provides a variety of phenomenological aspects, i.e., a fermion DM with an axion-like particle as the mediator. Axion-like particles (ALPs) are light pseudoscalar particles arising from extensions of the standard model. For example, the String/M theory framework generically provides a plethora of pseudoscalars due to the compactification process of the extra-dimensions [7, 8]. Since ALPs mainly interact with gauge bosons and fermions via dimension-five couplings, the main phenomenological aspects rely on the ALP-fermion and ALP-photon couplings. One could test the ALP-mediated models using particle colliders such as the beam dump experiments and rare mesons decay. Other interesting tests come from astrophysics such as the neutrino flux coming from supernova SN1987A, effects on stellar evolution of the horizontal branch of the HR-diagram and the number of relativistic degrees of freedom around the time of Big Bang Nucleosynthesis (BBN).

Recently, there has been interest in dark matter capturing in celestial objects such as neutron star (NS) and brown dwarf (BD) [9–12]. It has been shown that if the multiscattering effect is taken into account, the celestial objects accumulating dark matter are appealing targets for observation of DM annihilation. The DM-overdense objects then could be observed in 2 different ways depending on the lifetime of the mediator. If the mediator is short-lived and decays inside the celestial object, an extra energy would change

the energy budget and the DM can be observed through the lifetime and stability of the celestial objects. On the other hand, if the mediator has a sufficiently long enough lifetime such that it decays outside the celestial object, the situation allows us to probe DM via indirect detection.

In this work, we study ALP-mediated DM models using an effective Lagrangian approach. We then use the DM-nucleon cross-section to calculate the multiscatter capture rate of the celestial objects in the DM-rich region. We are interested in the case where ALP produced from annihilation has a sufficiently long lifetime such that the ALP decays into SM particles. Using the distribution of celestial objects near the Galactic Center and the DM generalized Navarro-Frenk-White (NFW) density profile, we are able to produce gamma-ray fluxes and neutrino fluxes from the DM annihilation in this model. The fluxes from neutrino produced from DM annihilation inside BDs could be detected via IceCube experiment and ANTARES neutrino telescope, whereas in the NS case, the neutrino fluxes are too low for any current observations. The gamma-ray fluxes from NSs and BDs can be tested against Fermi satellite and H.E.S.S. data. The constraints from gamma-ray observation using NSs and BDs as targets are able to rule out a significant portion of parameter space of coupling between ALP and fermions and the ALP mass. The constraints from gamma-ray fluxes perform better than the ones from neutrino fluxes due to the difference in the observed fluxes from the experiments.

## 2 Dark Matter Simplified Model

In this model, the SM is extended by a Dirac fermion,  $\chi$ , and a pseudoscalar ALP,  $a$ . The effective Lagrangian is given by

$$\mathcal{L} \supset \frac{1}{2} \partial_\mu a \partial^\mu a - \frac{1}{2} m_a^2 a^2 + \sum_f \frac{m_f}{f_a} C_f \bar{f} i \gamma_5 f a + \frac{m_\chi}{f_a} C_\chi \bar{\chi} i \gamma_5 \chi a - \frac{g_{a\gamma\gamma}}{4} F_{\mu\nu} \tilde{F}^{\mu\nu} a, \quad (2.1)$$

where  $f$  is any SM fermion with mass  $m_f$ , the masses of ALP and DM are  $m_a$  and  $m_\chi$ , respectively.  $F_{\mu\nu} = \partial_\mu A_\nu - \partial_\nu A_\mu$  is the  $U(1)_{\text{EM}}$  field strength tensor ( $\tilde{F}^{\mu\nu} = \frac{1}{2} \epsilon^{\mu\nu\alpha\beta} F_{\alpha\beta}$ ) and  $g_{a\gamma\gamma}$  is an effective ALP-photon coupling. For convenience, we define the effective ALP couplings by

$$g_{aff} = m_f C_f / f_a \quad \text{and} \quad g_{a\chi\chi} = m_\chi C_\chi / f_a. \quad (2.2)$$

In this model, we assume that ALP-fermion coupling  $C_f$  is universal for any fermion, i.e.,  $C_f$  and  $g_{aff} \propto m_f$ . The Dirac fermion  $\chi$  is assumed to be the DM particle. The ALP,  $a$ , acts as the mediator between SM and the hidden sector where  $g_{aff}$  acts as the connector coupling and  $g_{a\chi\chi}$  acts as the hidden sector coupling. Figure 1 shows the diagram of the scattering between DM and nucleons which is mediated by ALP and the diagrams of ALP decay into 2 photons and 2 SM particles (specifically neutrinos if kinematically allowed), respectively. The different regimes of interactions were studied for the freeze-in/out scenarios in [13–15], therefore we will not focus on the DM production mechanism in this paper.

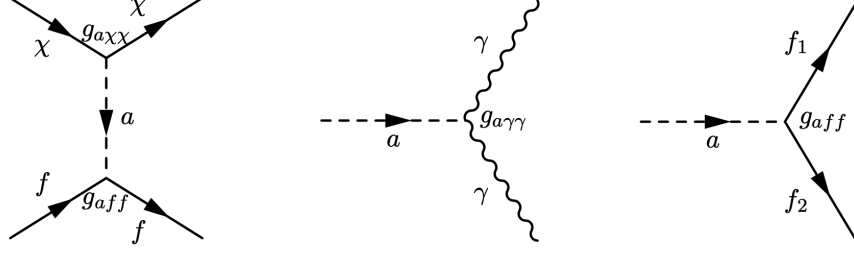


**Figure 1.** Diagrams a non-relativistic scattering of dark matter with the standard model where the ALP propagates an interaction (left), an ALP effectively decays into gamma-rays (middle) and an ALP effectively decays into SM particles (right).

As DM condenses around the celestial objects in the DM-rich region, the DM can fall into the objects by the mechanism called “dark matter multiscatter capture” [10, 16]. We will discuss this mechanism in the next section. DM can lose kinetic energy by scattering with the object’s components and falling into the celestial object. The scattering cross-section of  $\chi f \rightarrow \chi f$  in the low-energy limit is

$$\sigma(\chi f \rightarrow \chi f) = \frac{g_{aff}^2 g_{a\chi\chi}^2}{2\pi m_a^4} \frac{m_\chi^4 + m_f^4 + m_\chi^2 m_f^2}{(m_\chi + m_f)^2}. \quad (2.3)$$

Each time that DM scatters with the components of the object, DM will lose kinetic energy and move toward the center of the object. DM will then accumulate and start to annihilate inside the object producing a long-lived mediator which is an ALP. The lifetime of ALP decay into gamma-rays is given by

$$\tau_{a \rightarrow \gamma\gamma}^{-1} = \Gamma_{a \rightarrow \gamma\gamma} = \frac{1}{64\pi} g_{a\gamma\gamma}^2 m_a^3, \quad (2.4)$$

and the lifetime of ALP decay into SM particles is written as

$$\tau_{a \rightarrow ff}^{-1} = \Gamma_{a \rightarrow ff} = \frac{g_{aff}^2 n_f^c m_a}{8\pi} \sqrt{1 - \frac{4m_f^2}{m_a^2}}. \quad (2.5)$$

The probes on the ALP coupling have been studied in various methods (see [13, 17] for a review). For example, the astrophysical sources such as SN 1987A can provide us the constraints on ALP coupling that  $g_{a\gamma\gamma} < 6 \times 10^{-9} \text{ GeV}^{-1}$  for small ALP masses [18]. The red giant branch in several clusters [19] give the upper bounds on the ALP coupled to electrons as  $g_{aee} < 1.48 \times 10^{-13}$ , which is also similar to the analysis of the red giant in the Galactic globular cluster  $\omega$  Centauri  $g_{aee} < 1.3 \times 10^{-13}$  [20]. The ALP coupled to both SM and DM has been recently studied in the context of thermal history [13–15, 21, 22].

We are interested in the case that ALPs were generated by the DM annihilation from the celestial objects. We primarily aimed to constrain the ALP-SM coupling,  $g_{aff}$  from the gamma-rays and neutrinos observations. The celestial objects such as NSs and BDs are good targets since they are densely distributed around the Galactic Center where the DM density is generically higher.

### 3 Dark Matter Multiscatter Capture

DM from the Galactic halo can start to fall into the celestial object if the DM is sped up to the escape velocity of the object at the surface of the celestial body which is

$$v_{\text{esc}} = \sqrt{G_N M / R}, \quad (3.1)$$

where  $G_N$  is the gravitational constant,  $M$  and  $R$  are the total mass and the radius of the celestial body, respectively. As DM particles transit through the celestial body, they can scatter with stellar materials and lose their kinetic energy. Once the velocity of DM drops below the escape velocity of the celestial objects, DM is captured. The capturing process can occur via single or multiple scatters [9–11, 16, 23]. The probability for a given DM to undergo  $N$  scatter is given by

$$p_N(\tau) = 2 \int_0^1 dy \frac{y e^{y\tau} (y\tau)^N}{N!}, \quad (3.2)$$

where  $\tau = \frac{3}{2} \frac{\sigma_{\chi n}}{\sigma_{\text{sat}}}$  is the optical dept. The saturate cross-section is defined as  $\sigma_{\text{sat}} \equiv \pi R^2 / N_n$ , where  $N_n$  is the number of nucleons inside the celestial object. The meaning of saturation cross-section  $\sigma_{\text{sat}}$  is the threshold that guarantees that DM will scatter at least once. The probability can be approximated in the limit of single scatter ( $\tau \leq 1$ ) and multiple scatter ( $\tau \gg 1$ ) [10] as

$$p_N(\tau) \approx \begin{cases} \frac{2\tau^N}{N!(N+2)} + \mathcal{O}(\tau^{N+1}), & \text{if } \tau \leq 1 \\ \frac{2}{\tau^2} (N+1) \Theta(\tau - N). & \text{if } \tau \gg 1 \end{cases} \quad (3.3)$$

The capture rate after DM scattered  $N$  times and became trapped in the celestial object is given by

$$C_N(\tau) = \pi R^2 p_N(\tau) \frac{\sqrt{6} n_\chi}{3\sqrt{\pi} \bar{v}} \left( (2\bar{v}^2 + 3v_{\text{esc}}^2) - (2\bar{v}^2 + 3v_N^2) \exp\left(-\frac{3}{2} \frac{(2v_N^2 + 3v_{\text{esc}}^2)}{\bar{v}^2}\right) \right), \quad (3.4)$$

where  $n_\chi = \rho_\chi(r)/m_\chi$  is the local number density of DM and  $\bar{v}$  is the DM dispersion velocity. After scattering  $N$  times, the typical velocity of DM which takes into account the energy loss in each scattering is

$$v_N = v_{\text{esc}} \left( 1 - \frac{\beta_+}{2} \right)^{-N/2}, \quad (3.5)$$

where  $\beta_+ = 4m_\chi m_n / (m_\chi + m_n)^2$ . The total capture rate for a single celestial body is then given by

$$C = \sum_{N=1}^{\infty} C_N. \quad (3.6)$$

For sufficiently large  $N$ ,  $2\bar{v}^2 + 3v_N^2$  becomes much larger than  $\bar{v}_N^2$ , therefore, the exponential term in equation 3.4 can be neglected and the capture rate approaches  $C_N \rightarrow p_N(\tau) \times C_{\max}$ .  $C_{\max}$  is called the maximum capture rate (geometric capture rate) which is given by

$$C_{\max} = \pi R^2 n_\chi(r) v_0 \left( 1 + \frac{3}{2} \frac{v_{\text{esc}}^2}{\bar{v}(r)^2} \right), \quad (3.7)$$

where  $v_0 = \sqrt{8/3\pi\bar{v}}$ . This guarantees that the particles undergo a sufficiently large number of  $N$  scatters are captured.

Figure 2 shows the mass capture rate for a NS (left) with  $M_{\text{NS}} = 1.5 M_\odot$  and  $R_{\text{NS}} = 10$  km and a BD (right) with  $M_{\text{BD}} = 0.0378 M_\odot$  and  $R_{\text{BD}} = 69,911$  km as a function of nucleon scattering cross-section  $\sigma_{\chi n}$ . As  $\sigma_{\chi n}$  increases, the number of scatters  $N$  also increases, once it goes above the certain number of scatters that is sufficiently large enough to capture DM, the capture rate in equation 3.4 (black line) is approximately the maximum capture rate (red dash line) (equation 3.7). It can be seen that the BD capture rate is 100 times larger than the NS capture rate. This is because the effective radius of BD is much larger than the radius of NS, which causes more DM flux to pass through the object.

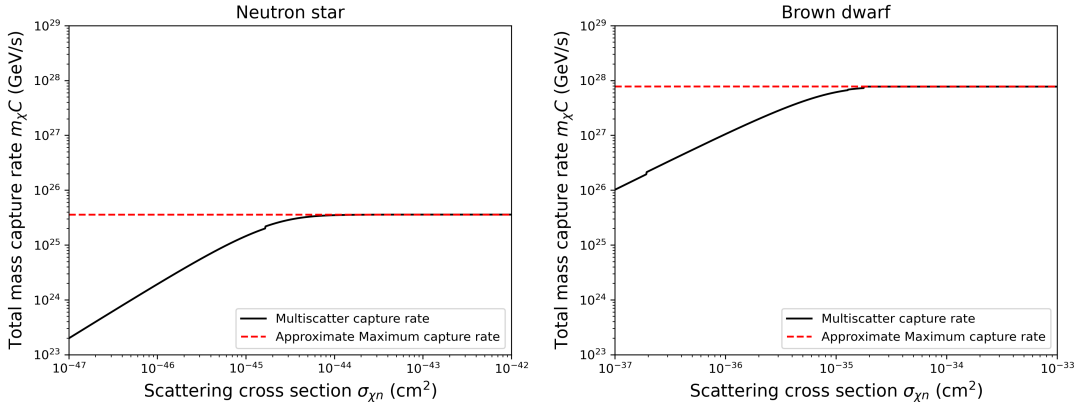


**Figure 2.** The mass capture rate  $m_\chi C$  as a function of nucleon scattering cross-section  $\sigma_{\chi n}$  for a NS and a BD. The red dash line indicates  $m_\chi C_{\max}$ . The DM model is applied with  $m_\chi = 10^3$  GeV,  $\rho_\chi = 0.42$  GeV/cm<sup>3</sup> and  $\bar{v} = 220$  km/s.

In order to calculate the total capture rate for all celestial objects within a given system (e.g. the Galactic Center or galaxy clusters), we need to take into account the number density of the objects within radii  $r_1$  and  $r_2$ , the total capture rate is

$$C_{\text{total}} = 4\pi \int_{r_1}^{r_2} r^2 n_\star(r) C dr, \quad (3.8)$$

where  $n_\star(r)$  is the number density of the celestial objects and  $C$  is the capture rate of a single object (equation 3.8). The number density of the celestial objects will be described in the following section.

## 4 The Galactic Center

In this section, we introduce the specific model of the DM velocity distribution and the target number density. The DM velocity dispersion and DM density affect the rate at which DM would fall into the gravitational potential and eventually fall into the object. At a given radius  $r$  from the Galactic Center, the dispersion velocity is

$$\bar{v} = \sqrt{3/2}v_c(r), \quad (4.1)$$

where  $v_c$  is the circular velocity at radius  $r$ , which depends on the total mass of the sphere of radius  $r$ :

$$v_c = \sqrt{G_N M(r)/r}. \quad (4.2)$$

We use the model for the mass distribution following reference [24]. This model has five components which are the central supermassive black holes  $M_{\text{BH}} = 4 \times 10^6 M_\odot$ , inner and outer bulges ( $\rho_{\text{inner}}$  and  $\rho_{\text{outer}}$ ), an disk component ( $\rho_{\text{disk}}$ ) and DM halo ( $\rho_{\text{DM}}$ ). Combining all five components, the total mass is

$$M(r) = M_{\text{BH}} + 4\pi \int_0^r r^2 (\rho_{\text{inner}} + \rho_{\text{outer}} + \rho_{\text{disk}} + \rho_{\text{DM}}) dr. \quad (4.3)$$

The DM generalized Navarro-Frenk-White (NFW) density profile [25] is

$$\rho_{\text{DM}} = \frac{\rho_0}{(r/r_s)^\gamma (1 + (r/r_s)^{1-\gamma})}, \quad (4.4)$$

where  $\rho_0 = 0.42 \text{ GeV/cm}^3$  is the local DM density, the scale radius is  $r_s = 12 \text{ kpc}$  and the slope index is ranging from  $\gamma = 1 - 1.5$ . The model of the inner bulge, outer bulge and disk is assumed to be an exponential sphere model:

$$\rho_i = \rho_{0,i} e^{-r/a_i}, \quad (4.5)$$

where the parameters of each component are shown in table 1.

Mass component	Total mass ( $M_\odot$ )	Scale radius (kpc)	Center density ( $M_\odot \text{ pc}^{-3}$ )
Inner bulge	$5 \times 10^7$	0.0038	$3.6 \times 10^4$
Outer bulge	$8.4 \times 10^9$	0.12	$1.9 \times 10^2$
Disk	$4.4 \times 10^{10}$	3.0	15

**Table 1.** Parameters in equation 4.5 for described the mass distribution of each component of the Galactic Center, from [24].

Neutron stars (NS) is the collapsed core of the massive star ( $10 - 25 M_\odot$ ), NS is composed almost entirely of degenerate neutrons with a mass ranging from  $1 - 1.5 M_\odot$  and a radius  $R_{\text{NS}} \simeq 10 \text{ km}$ . The number densities of NSs and black holes in regions around the Galactic Center have been numerically studied with the nuclear star cluster dynamics [26]. Two types of cluster models were described, ‘Fiducial’ and ‘Fiducial  $\times 10$ ’, both of which

are potentially good candidates for an NS distribution in the nuclear star clusters. The NS radial number density distribution from the ‘Fiducial  $\times 10$ ’ model is given by

$$n_{\text{NS}}(r) = \begin{cases} 5.98 \times 10^3 \left( \frac{r}{1 \text{ pc}} \right)^{-1.7} & \text{if } 0.1 \text{ pc} < r < 2 \text{ pc} \\ 2.08 \times 10^4 \left( \frac{r}{1 \text{ pc}} \right)^{-3.5} & \text{if } r > 2 \text{ pc} \end{cases}. \quad (4.6)$$

On the other hand, Brown dwarf (BD) is a failed star that is not massive enough to process the nuclear fusion of hydrogen into helium in its core. A huge amount of BDs are expected to be presented in our galaxy. The Milky Way may contain 25 – 100 billion BDs [27]. To obtain the radial distribution function of BDs, we follow the works in references [28, 29]. They extended the Kroupa Initial Mass Function (IMF) into the BD IMF which is described by the broken power law function,  $\frac{dN_{\text{BD}}}{dm} \propto m^{-\alpha}$ , where  $\alpha = 0.3$ ,  $N_{\text{BD}}$  is the number of BD and  $m$  is the mass of BD. The number density of the BDs with the mass range from  $0.01 - 0.07 M_{\odot}$  is given by

$$n_{\text{BD}}(r) = 7.5 \times 10^4 \left( \frac{r}{1 \text{ pc}} \right)^{-1.5}. \quad (4.7)$$

In our calculation, we will use the average mass of BDs as  $M_{\text{BD}} = 0.0378 M_{\odot}$  and their radius is assumed to be equal to the Jupiter radius  $R_{\text{BD}} = R_{\text{J}} = 69,911 \text{ km}$ .

## 5 Detection

Once DM becomes trapped in the celestial bodies (NS or BD), it has two possible fates. First, if DM does not self-annihilate, its density will rise near the core of the celestial object and it can lead to black hole formation and collapse. The second case is that the DM is annihilated with each other inside the celestial body. The evolution of the number of DM particles [23] inside an object  $N(t)$  is governed by an interplay between DM capture rate and DM annihilation rate, i.e.,

$$\frac{dN(t)}{dt} = C_{\text{total}} - C_A N(t)^2, \quad (5.1)$$

where  $C_{\text{total}}$  is the total capture rate (equation 3.8) and  $C_A = \langle \sigma_A v \rangle / V_{\text{eff}}$  is the average thermal annihilation cross-section over the effective volume of the celestial object body  $V_{\text{eff}} = 4\pi R_{\star}^3/3$ . The solution of equation 5.1 reads

$$N(t) = \sqrt{\frac{C_{\text{total}}}{C_A}} \tanh \frac{t}{t_{\text{eq}}}, \quad (5.2)$$

where  $t_{\text{eq}} = 1/\sqrt{C_A C_{\text{total}}}$  is the time scale required for the celestial object body to reach the DM equilibrium between capture and annihilation. Once it reaches the equilibrium,  $t > t_{\text{eq}}$ , the number of DM becomes time-independent, and the annihilation rate  $\Gamma_{\text{ann}}$  is simply

$$\Gamma_{\text{ann}} = \frac{C_{\text{total}}}{2}, \quad (5.3)$$

where the factor  $1/2$  comes from the fact that the DM annihilation process involves 2 DM particles. Since it has been shown that within the lifetime of the universe, the equilibrium between DM capturing rate and DM annihilation rate has already been reached for most of the parameter space [12], we will assume the above condition for our study. From equation 3.4, we know that the annihilation rate is proportional to the local DM density,  $\Gamma_{\text{ann}} \propto n_\chi$ , and the total capture rate (equation 3.8) is proportional to the number density of the celestial body,  $\Gamma_{\text{ann}} \propto n_\star$ , thus, the total annihilation rate is  $\Gamma_{\text{ann}} \propto n_\chi n_\star$ .

We consider the case in which DM annihilates into a long-lived ALP which weakly interacts with the matter such that it can escape from the celestial body and subsequently decay into a pair of SM particles. DM captured in celestial objects is expected to be annihilated with a small relative velocity, the mediator may be produced with the Lorentz boost factor  $\eta = m_\chi/m_a$ , where  $m_a$  is the mass of ALP. In order to calculate the sensitivities for the possible signals, we assume that the lifetime of the mediator,  $\tau$ , is sufficiently long such that the decay length exceeds the radius of the object  $R$ :

$$L = \eta c\tau > R. \quad (5.4)$$

The differential energy flux of gamma-ray arriving at Earth is given by [30]

$$E^2 \frac{d\Phi}{dE} = \frac{\Gamma_{\text{ann}}}{4\pi D^2} \times E^2 \frac{dN}{dE} \times \text{BR}(a \rightarrow \text{SM}) \times P_{\text{surv}}, \quad (5.5)$$

where  $D$  is the average distance from the target to Earth, in this case, the target is located around the Galactic Center, so  $D \approx 8$  kpc.  $\text{BR}(a \rightarrow \text{SM})$  is the branching ratio for the mediator into SM particles. For simplicity, we are assuming the unity of the branching ratio and the analysis is then separated into 2 cases, i.e., the spectrum of DM annihilates into a mediator and then decays into a pair of either 100% gamma-rays or 100% neutrinos. Their number distributions can be described by a box-shaped spectrum [31] which is given by

$$\frac{dN}{dE} = \frac{4}{\Delta E} \Theta(E - E_-) \Theta(E_+ - E), \quad (5.6)$$

where  $\Theta$  is Heaviside step function,  $\Delta E = E_+ - E_-$  is the width of the spectrum and  $E_\pm = (m_\chi/2) \left(1 \pm \sqrt{1 - m_a^2/m_\chi^2}\right)$ . The probability of the mediator,  $a$ , decaying outside the celestial object is

$$P_{\text{surv}} = e^{-R/\eta c\tau} - e^{-D/\eta c\tau}. \quad (5.7)$$

An example of the survival probability as a function of the decay length  $\eta c\tau$  is shown in figure 3. The plot shows the survival probability of the SM particle produced by the mediator at the distance  $\eta c\tau$  from a NS. The probability is taken with the assumption that the SM particle does not reach the Earth if the mediator decays inside the star (red dash line), i.e., for  $\eta c\tau < R_\star$ , the probability is assumed to be zero. In this work, we will consider the maximally optimistic case where we take  $P_{\text{surv}} = 1$  for both gamma-rays and neutrinos cases. Furthermore, we also calculate the bounds of an effective ALP-photon coupling and an effective ALP-SM coupling for ALPs that decay in the distance between the object's surface and the Earth. The bound on  $g_{a\gamma\gamma}$  are calculated from the lifetime in equation 2.4

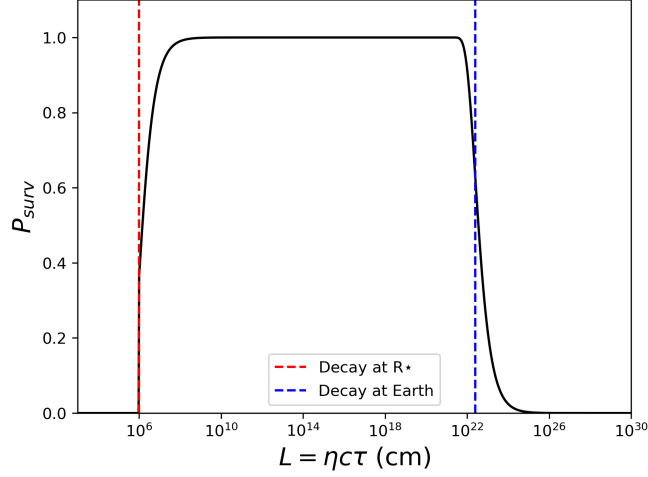


**Figure 3.** The plot shows the probability of the SM particle surviving from the NS to the detector at the Earth.

and the result is shown in the left panel of figure 4. We found that for the lower mass of ALP, the  $g_{a\gamma\gamma}$  has already been excluded by the constraint from the helioscope CAST (CERN Axion Solar Telescope) [32–35]. Therefore for the ALP decaying into 100% photons case, we will aim to study for ALP mass range higher than  $10^{-9}$  GeV. In the 100% decaying into neutrinos case, the bound on  $g_{aff}$  is calculated with the lifetime from equation 2.5. The result is shown in the right panel of figure 4 where  $m_f = m_\nu = 0.1$  eV is assumed. We only show the bound from BD because it is the only target that can generate sufficient fluxes of neutrinos that are detectable by the experiments, which we will discuss shortly.

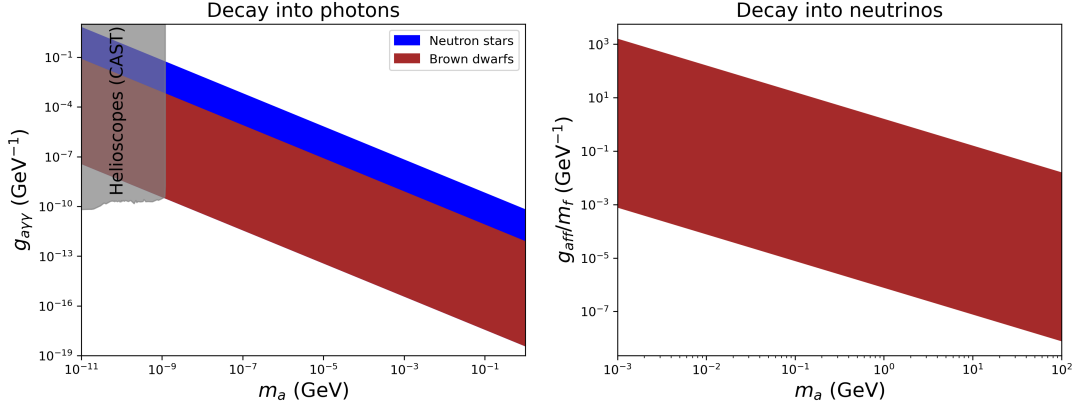


**Figure 4.** The left panel shows the bounds on an effective ALP-photon coupling for an ALP decay between the object’s surface and the Earth. We also display the bounds from CAST helioscopes in the grey region. The right panel shows the bounds on an effective ALP-SM coupling for an ALP decay between the object’s surface and the Earth, where in this case ALP decays into neutrinos.

In order to set the limits on the ALP coupling, We use the Galactic Center measured fluxes from various observations. The gamma-ray fluxes are taken from Fermi and H.E.S.S.

and the details of the data analysis are given in [36]. Fermi data is used for the model fluxes with energy less than 100 GeV [37], and we use H.E.S.S. [38] to set limits around TeV scale. The high energy neutrino fluxes were taken from IceCube [39] and ANTARES [40] where they have the upper limits on the muon neutrinos flux from the direction of the Galactic Center ( $-40^\circ < l < 40^\circ$  and  $-3^\circ < b < 3^\circ$  in Galactic Coordinate) in the energy range between 1 TeV and 1 PeV. We set the limits by requiring that the maximum value of the DM fluxes must not exceed the measurable fluxes from the observation. This can be done by determining the ALP coupling  $g_{aff}$  for each energy bin ( $E \approx m_\chi$ ) which gives the highest possible scattering cross-section (equation 2.3) providing the energy flux (equation 5.5) below the measured flux.

To generate the gamma-ray energy spectra, we use *Asteria* [22] to calculate the total DM capture rate. We use the number density of NSs from equation 4.6 and the number density of BDs from equation 4.7. We integrate both densities over the spherical shell between radius  $r_1 = 0.1$  pc and  $r_2 = 100$  pc. Choosing  $r_1 = 0.1$  pc to avoid poor modeling of the DM cusp-like profile at the Galactic Center. The outer radius  $r_2 = 100$  pc is chosen due to the fact that NSs/BDs number density falls rapidly outside this region. We assume that the ALP decays into 100% photons and  $P_{\text{surv}} = 1$  for simplicity. We show the largest possible signal for different choices of density slope index  $\gamma = 1, 1.5$  in the NFW DM profile in figure 5 along with the measured gamma-ray flux from Fermi (black) and H.E.S.S. (blue). For NSs, one could expect that only the gamma-rays from the NFW DM profile with  $\gamma = 1.5$  are detectable by H.E.S.S. data. For BDs, both gamma-rays from slope index  $\gamma = 1, 1.5$  are higher than the measured fluxes from Fermi and H.E.S.S., which would give us strong constraints to the ALP coupling.

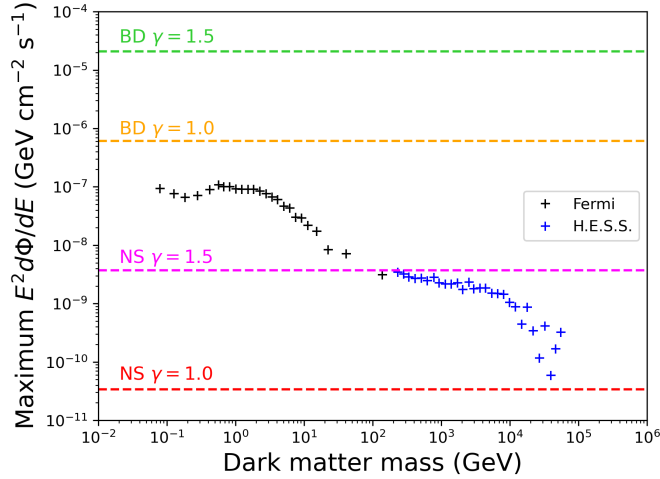


**Figure 5.** Maximum differential fluxes of gamma-ray of the NSs or BDs from the Galactic Center. The gamma-ray fluxes from the Galactic Center observed by Fermi and H.E.S.S. are shown in black and blue, respectively.

To generate the neutrino spectra, we follow the same procedure as the gamma-rays spectra. The largest possible fluxes for  $\gamma = 1, 1.5$  are shown in figure 6 along with the

measured neutrino fluxes from IceCube (blue) and ANTARES (black). We find that the maximum flux from the NS is lower than the observation fluxes by approximately 2 orders of magnitude. As a result, we will study only BDs as the potential sources of neutrino flux.

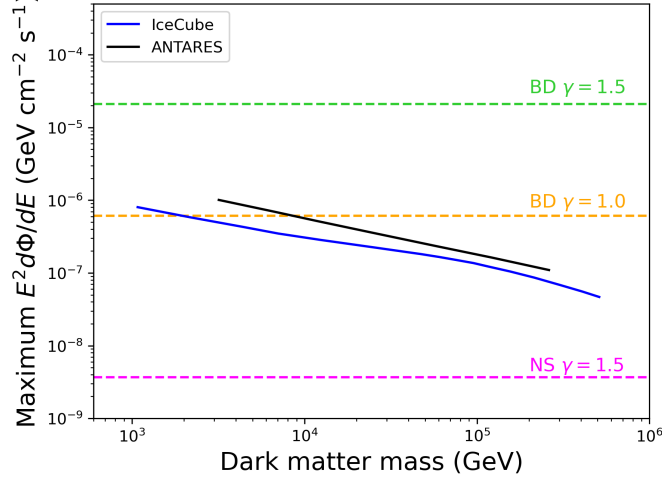


**Figure 6.** Maximum differential fluxes of neutrino from the NSs in the Galactic Center. The neutrino fluxes from the Galactic Center observed by IceCube and ANTARES are shown in blue and black, respectively.

## 6 Results

Figure 7 shows our constraints on an effective ALP coupling for DM-SM scattering mediated by ALP. The gamma-rays were produced by the production of DMs that annihilated inside the object,  $\chi\chi \rightarrow a$ ,  $a \rightarrow \gamma\gamma$ . The limits were placed on  $E^2 d\Phi/dE$  with the gamma-ray observatories (Fermi and H.E.S.S.). Our calculation on gamma-ray flux has been described in the previous section and the other parameters in the plot are  $g_{a\chi\chi} = 1 \times 10^{-3}$  and  $m_a = m_\chi/10^5$ . The bounds from our works are displayed along with the other constraints. The Fermi upper limit is shown in black for BD targets and the H.E.S.S. upper limit using NSs and BDs as targets are shown in blue and red, respectively. We show the results of BDs for  $\gamma = 1$  in the dash line and  $\gamma = 1.5$  in the solid line. Since we concentrate on the simplest case where  $C_f$  is universal, therefore the result we present is in the form of  $g_{aff}/m_f = C_f/f_a$ , where  $m_f$  is the mass of the fermion. In the gamma-rays final state, we use proton and neutron mass for calculating the scattering cross section, therefore  $m_f = m_n \approx m_p$ . For NSs, we show only  $\gamma = 1.5$  since the gamma-ray flux is detectable only at H.E.S.S. Our results show that the limits in this work are significantly stronger than previously existing constraints. For higher masses, NSs provide stronger bounds than BDs since NSs require a lower cross-section to capture the DM (figure 2).

The other constraints in the figure 7 are the following. The constraints of the study of the supernova SN 1987A can provide strong constraints [18] and recently updated in reference [41]. Considering the cooling of the horizontal branch (HB) stars provides the parameters space of ALPs [42]. The exclusion bounds for the decay of  $K^+ \rightarrow \pi^+ + \text{inv.}$

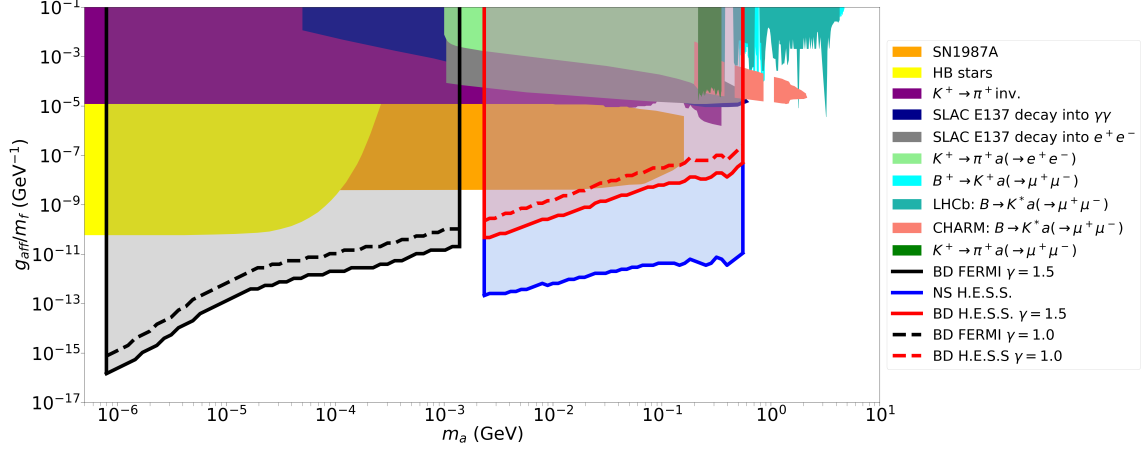


**Figure 7.** The constraints plot on the ALP-fermion coupling,  $g_{aff}$  as a function of  $m_a$ . The results of our work are shown in black, red and blue for BDs focused on Fermi, BDs focused on H.E.S.S. and NSs focused on H.E.S.S., respectively. Other constraints were briefly discussed in the text (see [13] for a review).

from NA62 [43] are given in the form of branching ratio. The strong constraints come from the electron beam dump experiment SLAC E137 [44], ALPs can be produced by the bremsstrahlung, positrons annihilation, or Primakoff effect.  $K^+ \rightarrow \pi^+ a(\rightarrow e^+e^-)$  from NA 48/2 [45] provide C.L. 90% upper limits.  $B^+ \rightarrow K^+ a(\rightarrow \mu^+\mu^-)$  from LHCb [46] provide C.L. 95% upper limits on the branching ratio as a function of the lifetime of  $a$ .  $B \rightarrow K^* a(\rightarrow \mu^+\mu^-)$  from LHCb [47] also provide the 95% C.L. upper limit on the branching ratio as a function of the mass and lifetime of  $a$ . The limits from  $B \rightarrow K^* a(\rightarrow \mu^+\mu^-)$  at fixed target come from CHARM [48].  $K^+ \rightarrow \pi^+ a(\rightarrow \mu^+\mu^-)$  from NA 48/2 [49] provide C.L. 90% upper limits on the branching ratio as a function of lifetime of  $a$ . From the work of [13] where they have studied the model of the production of ALP-mediated DM in the thermal scenarios, our work (small  $g_{a\chi\chi}$  and  $g_{aff}$ ) corresponds to the case that dark matter is produced by freeze-in and the ALP may or may not be in equilibrium with the SM. Therefore, viable parameter space for the freeze-in scenario is not ruled out by our study.

We also show results when we vary the ratio of the mass of DM and ALP in figure 8. The constraints on  $g_{aff}$  NS as the targets are calculated with  $g_{a\chi\chi} = 1 \times 10^{-3}$  and the mass ratios  $m_a = m_\chi/10^4$ ,  $m_a = m_\chi/10^5$  and  $m_a = m_\chi/10^6$  are shown in blue, red and black, respectively. The results show that the decreasing of the mass ratio gives stronger bounds in the lower masses region of ALP.

Figure 9 shows the upper limits on the ALP-fermion coupling from the neutrino observations (IceCube and ANTARES). The neutrino fluxes were generated by only focusing on BD as the targets as discussed in the earlier section. The bounds are weaker than the gamma-ray case but still stronger than existing constraints, especially in the higher ALP mass region. Under the universal ALP-fermion coupling assumption, the region where ALP decays en route (figure 4) can be constrained to be  $m_a \gtrsim 0.6$  GeV.

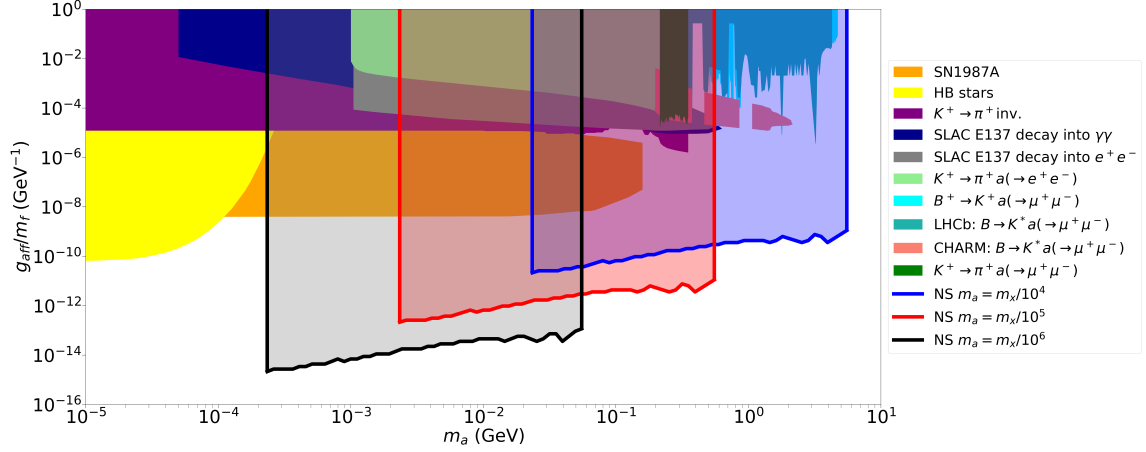


**Figure 8.** The constraints plot on the ALP-fermion coupling where we fixed the  $g_{a\chi\chi} = 1 \times 10^{-3}$ . We only focused on the NSs as the only sources. We show the results for the mass  $m_a = m_\chi/10^4$ ,  $m_a = m_\chi/10^5$  and  $m_a = m_\chi/10^6$  in blue, red and black, respectively.

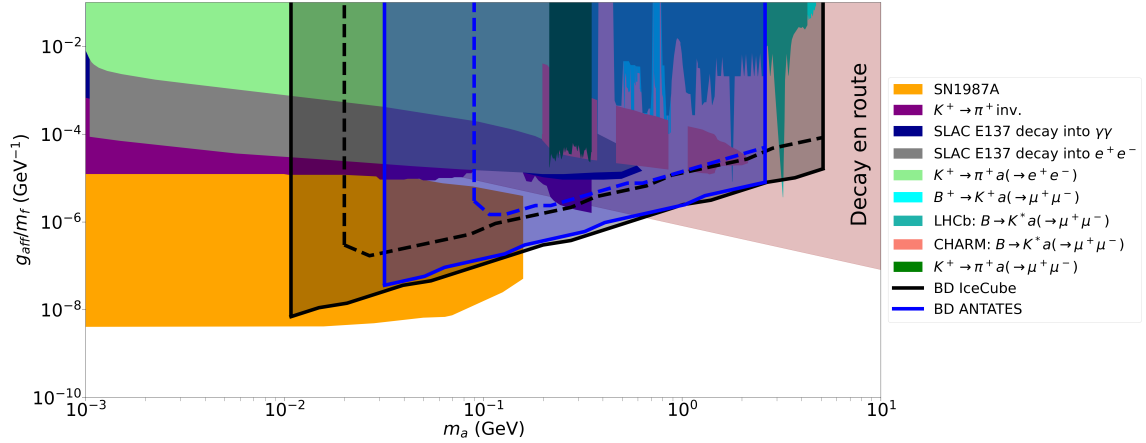


**Figure 9.** The constraints plot from the neutrino observations on the ALP-fermion coupling,  $g_{aff}$  as a function of  $m_a$  where we fixed the ALP-DM coupling as  $g_{a\chi\chi} = 1 \times 10^{-3}$  and  $m_a = m_\chi/10^5$ . The NFW DM profiles with  $\gamma = 1, 1.5$  are represented in dash and solid lines, respectively.

## 7 Conclusion

In this work, we have studied the constraints of the ALP-mediated DM models from celestial objects such as neutron stars (NS) and brown dwarfs (BD). The DM can be captured in celestial objects where the DM accumulation process is controlled by the dark matter multiscatter capture mechanism. The annihilation of DM inside the objects produces the long-lived ALPs which will decay into the SM particles outside the objects. We study the case that ALP decays into gamma-rays and neutrinos separately and compare the fluxes with data from observation. For gamma-ray fluxes, we present our results on  $g_{aff}/m_f$  in figure 7. The results show the strong bounds that can rule out a significant portion of the parameter space. We point out that by using NSs as targets the model provides

a stronger bound than BD ones due to the lower fluxes required to match with H.E.S.S. data. For Fermi data with the lower DM mass range, only BDs are detectable via the gamma-ray channel. We also present the upper bounds for different mass ratios in figure 8 and show that our limits are generally stronger than existing constraints across the mass range of ALP. The results for neutrino fluxes are present in figure 9. We found that the only possible targets that can produce sufficient neutrino flux are BDs. With data from IceCube and ANTARES, we can probe our model with the higher mass range. Similar to the gamma-ray channel, the bounds from neutrino fluxes are also generally stronger than the previous constraints on ALP. Provided that ALP decays en route towards the Earth, the allowed parameter space for this model is strictly constrained with  $m_a \gtrsim 0.6$  GeV. This emphasizes the importance of the next-generation probes of the neutrino fluxes at higher energies such as ARIANNA, ARIA, IceCube-Gen2 [50, 51], KM3Net [52], ANITA-IV [53], PUEO [54], RNO-G [55] and Auger [56].

For future works, we are interested in exploring the phenomenological consequences of the possibility that ALP decays inside celestial objects providing additional energy to their internal processes. We also would like to investigate the effects of ALP-mediated interactions on the nuclear equation of state (EoS) and neutron star stability.

## Acknowledgement

TK and CP have been supported by the National Astronomical Research Institute of Thailand (NARIT). CP is supported by Fundamental Fund 2566 of Khon Kaen University and Research Grant for New Scholar, Office of the Permanent Secretary, Ministry of Higher Education, Science, Research and Innovation under contract no. RGNS64-043. We thank Areef Waeming and Daris Samart for their helpful comments and discussions.

## References

- [1] B. Patt and F. Wilczek, *Higgs-field portal into hidden sectors*, [hep-ph/0605188](#).
- [2] J. March-Russell, S. M. West, D. Cumberbatch, and D. Hooper, *Heavy Dark Matter Through the Higgs Portal*, *JHEP* **07** (2008) 058, [[arXiv:0801.3440](#)].
- [3] A. Djouadi, A. Falkowski, Y. Mambrini, and J. Quevillon, *Direct Detection of Higgs-Portal Dark Matter at the LHC*, *Eur. Phys. J. C* **73** (2013), no. 6 2455, [[arXiv:1205.3169](#)].
- [4] A. Falkowski, J. Juknevich, and J. Shelton, *Dark Matter Through the Neutrino Portal*, [arXiv:0908.1790](#).
- [5] M. Escudero, N. Rius, and V. Sanz, *Sterile neutrino portal to Dark Matter I: The  $U(1)_{B-L}$  case*, *JHEP* **02** (2017) 045, [[arXiv:1606.01258](#)].
- [6] M. Escudero, N. Rius, and V. Sanz, *Sterile Neutrino portal to Dark Matter II: Exact Dark symmetry*, *Eur. Phys. J. C* **77** (2017), no. 6 397, [[arXiv:1607.02373](#)].
- [7] P. Svrcek and E. Witten, *Axions In String Theory*, *JHEP* **06** (2006) 051, [[hep-th/0605206](#)].
- [8] A. Arvanitaki, S. Dimopoulos, S. Dubovsky, N. Kaloper, and J. March-Russell, *String Axiverse*, *Phys. Rev. D* **81** (2010) 123530, [[arXiv:0905.4720](#)].

- [9] B. Dasgupta, A. Gupta, and A. Ray, *Dark matter capture in celestial objects: Improved treatment of multiple scattering and updated constraints from white dwarfs*, *JCAP* **08** (2019) 018, [[arXiv:1906.04204](#)].
- [10] C. Ilie, J. Pilawa, and S. Zhang, *Comment on “Multiscatter stellar capture of dark matter”*, *Phys. Rev. D* **102** (2020), no. 4 048301, [[arXiv:2005.05946](#)].
- [11] C. Ilie and C. Levy, *Multicomponent multiscatter capture of dark matter*, *Phys. Rev. D* **104** (2021), no. 8 083033, [[arXiv:2105.09765](#)].
- [12] T. T. Q. Nguyen and T. M. P. Tait, *Bounds on Long-lived Dark Matter Mediators from Neutron Stars*, [arXiv:2212.12547](#).
- [13] A. Bharucha, F. Brümmer, N. Desai, and S. Mutzel, *Axion-like particles as mediators for dark matter: beyond freeze-out*, *JHEP* **02** (2023) 141, [[arXiv:2209.03932](#)].
- [14] D. K. Ghosh, A. Ghoshal, and S. Jeusun, *Axion-like particle (ALP) portal freeze-in dark matter confronting ALP search experiments*, [arXiv:2305.09188](#).
- [15] J. A. Dror, S. Gori, and P. Munbodh, *QCD axion-mediated dark matter*, *JHEP* **09** (2023) 128, [[arXiv:2306.03145](#)].
- [16] J. Bramante, A. Delgado, and A. Martin, *Multiscatter stellar capture of dark matter*, *Phys. Rev. D* **96** (2017), no. 6 063002, [[arXiv:1703.04043](#)].
- [17] M. J. Dolan, T. Ferber, C. Hearty, F. Kahlhoefer, and K. Schmidt-Hoberg, *Revised constraints and Belle II sensitivity for visible and invisible axion-like particles*, *JHEP* **12** (2017) 094, [[arXiv:1709.00009](#)]. [Erratum: *JHEP* 03, 190 (2021)].
- [18] J. Jaeckel, P. C. Malta, and J. Redondo, *Decay photons from the axionlike particles burst of type II supernovae*, *Phys. Rev. D* **98** (2018), no. 5 055032, [[arXiv:1702.02964](#)].
- [19] O. Straniero, C. Pallanca, E. Dalessandro, I. Dominguez, F. R. Ferraro, M. Giannotti, A. Mirizzi, and L. Piersanti, *The RGB tip of galactic globular clusters and the revision of the axion-electron coupling bound*, *Astron. Astrophys.* **644** (2020) A166, [[arXiv:2010.03833](#)].
- [20] F. Capozzi and G. Raffelt, *Axion and neutrino bounds improved with new calibrations of the tip of the red-giant branch using geometric distance determinations*, *Phys. Rev. D* **102** (2020), no. 8 083007, [[arXiv:2007.03694](#)].
- [21] C. Balázs et al., *Cosmological constraints on decaying axion-like particles: a global analysis*, *JCAP* **12** (2022) 027, [[arXiv:2205.13549](#)].
- [22] R. K. Leane and J. Smirnov, *Dark Matter Capture in Celestial Objects: Treatment Across Kinematic and Interaction Regimes*, [arXiv:2309.00669](#).
- [23] C. Kouvaris and P. Tinyakov, *Can Neutron stars constrain Dark Matter?*, *Phys. Rev. D* **82** (2010) 063531, [[arXiv:1004.0586](#)].
- [24] Y. Sofue, *Rotation Curve and Mass Distribution in the Galactic Center — From Black Hole to Entire Galaxy —*, *Publ. Astron. Soc. Jap.* **65** (2013) 118, [[arXiv:1307.8241](#)].
- [25] J. F. Navarro, C. S. Frenk, and S. D. M. White, *The Structure of cold dark matter halos*, *Astrophys. J.* **462** (1996) 563–575, [[astro-ph/9508025](#)].
- [26] A. Generozov, N. C. Stone, B. D. Metzger, and J. P. Ostriker, *An overabundance of black hole X-ray binaries in the Galactic Centre from tidal captures*, *Mon. Not. Roy. Astron. Soc.* **478** (2018), no. 3 4030–4051, [[arXiv:1804.01543](#)].

- [27] K. Mužić, R. Schödel, A. Scholz, V. C. Geers, R. Jayawardhana, J. Ascenso, and L. A. Cieza, *The low-mass content of the massive young star cluster RCW 38*, *Monthly Notices of the Royal Astronomical Society* **471** (07, 2017) 3699–3712, [<https://academic.oup.com/mnras/article-pdf/471/3/3699/19530209/stx1906.pdf>].
- [28] P. Kroupa, C. Weidner, J. Pflamm-Altenburg, I. Thies, J. Dabringhausen, M. Marks, and T. Maschberger, *The stellar and sub-stellar IMF of simple and composite populations*, [arXiv:1112.3340](https://arxiv.org/abs/1112.3340).
- [29] P. Amaro-Seoane, *Extremely large mass-ratio inspirals*, *Phys. Rev. D* **99** (2019), no. 12 123025, [[arXiv:1903.10871](https://arxiv.org/abs/1903.10871)].
- [30] R. K. Leane, K. C. Y. Ng, and J. F. Beacom, *Powerful Solar Signatures of Long-Lived Dark Mediators*, *Phys. Rev. D* **95** (2017), no. 12 123016, [[arXiv:1703.04629](https://arxiv.org/abs/1703.04629)].
- [31] A. Ibarra, S. Lopez Gehler, and M. Pato, *Dark matter constraints from box-shaped gamma-ray features*, *JCAP* **07** (2012) 043, [[arXiv:1205.0007](https://arxiv.org/abs/1205.0007)].
- [32] **CAST** Collaboration, E. Arik et al., *Probing eV-scale axions with CAST*, *JCAP* **02** (2009) 008, [[arXiv:0810.4482](https://arxiv.org/abs/0810.4482)].
- [33] **CAST** Collaboration, S. Aune et al., *CAST search for sub-eV mass solar axions with  $^3\text{He}$  buffer gas*, *Phys. Rev. Lett.* **107** (2011) 261302, [[arXiv:1106.3919](https://arxiv.org/abs/1106.3919)].
- [34] **CAST** Collaboration, M. Arik et al., *Search for Solar Axions by the CERN Axion Solar Telescope with  $^3\text{He}$  Buffer Gas: Closing the Hot Dark Matter Gap*, *Phys. Rev. Lett.* **112** (2014), no. 9 091302, [[arXiv:1307.1985](https://arxiv.org/abs/1307.1985)].
- [35] **CAST** Collaboration, V. Anastassopoulos et al., *New CAST Limit on the Axion-Photon Interaction*, *Nature Phys.* **13** (2017) 584–590, [[arXiv:1705.02290](https://arxiv.org/abs/1705.02290)].
- [36] D. Malyshev, M. Chernyakova, A. Neronov, and R. Walter, *Leptonic origin of the 100 MeV  $\gamma$ -ray emission from the Galactic centre*, *Astron. Astrophys.* **582** (2015) A11, [[arXiv:1503.05120](https://arxiv.org/abs/1503.05120)].
- [37] **Fermi-LAT** Collaboration, F. Acero et al., *Fermi Large Area Telescope Third Source Catalog*, *Astrophys. J. Suppl.* **218** (2015), no. 2 23, [[arXiv:1501.02003](https://arxiv.org/abs/1501.02003)].
- [38] **H.E.S.S.** Collaboration, A. Abramowski et al., *Acceleration of petaelectronvolt protons in the Galactic Centre*, *Nature* **531** (2016) 476, [[arXiv:1603.07730](https://arxiv.org/abs/1603.07730)].
- [39] **IceCube** Collaboration, M. G. Aartsen et al., *Constraints on Galactic Neutrino Emission with Seven Years of IceCube Data*, *Astrophys. J.* **849** (2017), no. 1 67, [[arXiv:1707.03416](https://arxiv.org/abs/1707.03416)].
- [40] **ANTARES** Collaboration, S. Adrian-Martinez et al., *Constraints on the neutrino emission from the Galactic Ridge with the ANTARES telescope*, *Phys. Lett. B* **760** (2016) 143–148, [[arXiv:1602.03036](https://arxiv.org/abs/1602.03036)].
- [41] S. Hoof and L. Schulz, *Updated constraints on axion-like particles from temporal information in supernova SN1987A gamma-ray data*, *JCAP* **03** (2023) 054, [[arXiv:2212.09764](https://arxiv.org/abs/2212.09764)].
- [42] D. Cadamuro and J. Redondo, *Cosmological bounds on pseudo Nambu-Goldstone bosons*, *JCAP* **02** (2012) 032, [[arXiv:1110.2895](https://arxiv.org/abs/1110.2895)].
- [43] **NA62** Collaboration, E. Cortina Gil et al., *Measurement of the very rare  $K^+ \rightarrow \pi^+ \nu \bar{\nu}$  decay*, *JHEP* **06** (2021) 093, [[arXiv:2103.15389](https://arxiv.org/abs/2103.15389)].
- [44] J. D. Bjorken, S. Ecklund, W. R. Nelson, A. Abashian, C. Church, B. Lu, L. W. Mo, T. A.

- Nunamaker, and P. Rassmann, *Search for Neutral Metastable Penetrating Particles Produced in the SLAC Beam Dump*, *Phys. Rev. D* **38** (1988) 3375.
- [45] **NA48/2** Collaboration, J. R. Batley et al., *Precise measurement of the  $K^{+-} \rightarrow \pi^{+} e^{-} e^{-}$  decay*, *Phys. Lett. B* **677** (2009) 246–254, [[arXiv:0903.3130](#)].
  - [46] **LHCb** Collaboration, R. Aaij et al., *Search for long-lived scalar particles in  $B^{+} \rightarrow K^{+} \chi(\mu^{+} \mu^{-})$  decays*, *Phys. Rev. D* **95** (2017), no. 7 071101, [[arXiv:1612.07818](#)].
  - [47] **LHCb** Collaboration, R. Aaij et al., *Search for hidden-sector bosons in  $B^0 \rightarrow K^{*0} \mu^{+} \mu^{-}$  decays*, *Phys. Rev. Lett.* **115** (2015), no. 16 161802, [[arXiv:1508.04094](#)].
  - [48] B. Döbrich, F. Ertas, F. Kahlhoefer, and T. Spadaro, *Model-independent bounds on light pseudoscalars from rare B-meson decays*, *Phys. Lett. B* **790** (2019) 537–544, [[arXiv:1810.11336](#)].
  - [49] **NA48/2** Collaboration, J. R. Batley et al., *Searches for lepton number violation and resonances in  $K^{\pm} \rightarrow \pi \mu \mu$  decays*, *Phys. Lett. B* **769** (2017) 67–76, [[arXiv:1612.04723](#)].
  - [50] **IceCube-Gen2** Collaboration, M. G. Aartsen et al., *IceCube-Gen2: the window to the extreme Universe*, *J. Phys. G* **48** (2021), no. 6 060501, [[arXiv:2008.04323](#)].
  - [51] **IceCube** Collaboration, A. Ishihara, *The IceCube Upgrade - Design and Science Goals*, *PoS ICRC2019* (2021) 1031, [[arXiv:1908.09441](#)].
  - [52] **KM3Net** Collaboration, S. Adrian-Martinez et al., *Letter of intent for KM3NeT 2.0*, *J. Phys. G* **43** (2016), no. 8 084001, [[arXiv:1601.07459](#)].
  - [53] **ANITA** Collaboration, P. W. Gorham et al., *Constraints on the ultrahigh-energy cosmic neutrino flux from the fourth flight of ANITA*, *Phys. Rev. D* **99** (2019), no. 12 122001, [[arXiv:1902.04005](#)].
  - [54] **PUEO** Collaboration, Q. Abarr et al., *The Payload for Ultrahigh Energy Observations (PUEO): a white paper*, *JINST* **16** (2021), no. 08 P08035, [[arXiv:2010.02892](#)].
  - [55] **RNO-G** Collaboration, J. A. Aguilar et al., *Design and Sensitivity of the Radio Neutrino Observatory in Greenland (RNO-G)*, *JINST* **16** (2021), no. 03 P03025, [[arXiv:2010.12279](#)]. [Erratum: *JINST* **18**, E03001 (2023)].
  - [56] **Pierre Auger** Collaboration, A. Aab et al., *Probing the origin of ultra-high-energy cosmic rays with neutrinos in the EeV energy range using the Pierre Auger Observatory*, *JCAP* **10** (2019) 022, [[arXiv:1906.07422](#)].